

Structural analysis of impact-related deformation in the collar rocks of the Vredefort Dome, South Africa

Frank Wieland

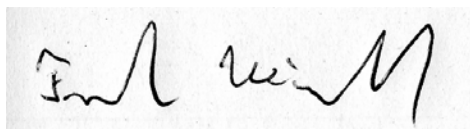
*School of Geosciences
University of the Witwatersrand*

Thesis submitted to the Faculty of Science, University of the Witwatersrand, Johannesburg, South Africa, in fulfilment of the requirements for the degree of Doctor of Philosophy.

Johannesburg, 2006

Declaration

I declare that this research is my own work. It is being submitted for the degree of Doctor of Philosophy at the University of the Witwatersrand, Johannesburg, South Africa. It has not been submitted before for any degree or examination in any other University.



Frank Wieland

_____ day of _____ 2006.

Abstract

The Vredefort Dome is located southwest of Johannesburg, South Africa, and represents the deeply eroded remnant of the central uplift of the world's largest known impact structure, with an estimated diameter of ~300 km. The Vredefort impact structure is also the oldest known impact structure on Earth (~2.02 Ga). The Vredefort Dome comprises an ~40 km wide core of Archaean basement gneisses and an ~20 km wide collar of subvertical to overturned Late Archaean to Palaeoproterozoic supracrustal strata.

This project presents the results of Landsat-TM and aerial photograph analysis, as well as field mapping of Witwatersrand Supergroup metasedimentary strata in the collar of the Vredefort Dome. The aim of this study was to investigate the structures (such as folds, faults, fractures), at all scales, and other deformation features (such as shatter cones and pseudotachylitic breccias) in the field area, and to establish geometric and temporal relationships between these features with regard to the impact cratering process. This study revealed a highly heterogeneous internal structure of the collar involving folds, faults, fractures and melt breccias that are interpreted as the product of shock deformation and central uplift formation during the Vredefort impact event. Broadly radially-oriented symmetric and asymmetric folds, with wavelengths from tens of metres to kilometres, and conjugate radial to oblique faults with strike-slip displacements of, typically, tens to hundreds of metres accommodated tangential shortening of the collar of the dome that decreased from ~17 %, at a radial distance from the dome centre of 21 km, to <5 % at a radial distance of 29 km. Ubiquitous shear fractures containing pseudotachylitic breccia, particularly in the metapelitic units, display variable local slip senses consistent with either tangential shortening or tangential extension; however, it is uncertain whether they formed at the same time as the larger faults during the rise of the central uplift or earlier, during the shock compression phase of cratering.

Contrary to the findings about shatter cones of some earlier workers in the Vredefort structure, the Vredefort cone fractures do not show uniform apex orientations at any given outcrop, nor do small cones show a pattern consistent with the previously postulated "master cone" concept. The model of simple back-rotation of the strata to a horizontal pre-impact position also does not lead to a uniform centripetal-upward orientation of the cone apices. Striation patterns on the cone surfaces are variable, ranging from typically diverging, i.e., branching off the cone

apex, to subparallel to parallel on almost flat surfaces. Striation angles on shatter cones do not increase with distance from the crater centre, as suggested previously. Instead, individual outcrops present a range of such striation angles, and a more irregular distribution of striation angle values with regard to the distance from the crater centre suggests localised controls involving the nature and shape of various heterogeneities in the target rock on this aspect of cone morphology.

On the basis of the observations made during this study on small-scale structures in the collar of the Vredefort Dome, the relationship of shatter cones with curvilinear fractures (multi-striated joint sets - MSJS) is confirmed. Pervasive, metre-scale tensile fractures crosscut shatter cones and appear to have formed after the closely-spaced MSJ-type fractures. The results of this study indicate that none of the existing models is able to explain all characteristics of shatter cones fully; therefore, a combination of aspects of the different models may currently be the best possible way to explain the formation and origin of shatter cones, and the formation of the related MSJ and their characteristic aspects (e.g., curvilinear shape, melt formation, etc.). The observed variety of shatter cone orientations, surface morphology and striation geometry in the dome concurs broadly with the results of some previous studies. The abundance of striated surfaces along closely-spaced sets of fractures (MSJ) observed in this study can be reconciled with reflection/scattering of a fast propagating wave at heterogeneities in the target rocks, as proposed by recent studies. This would mean that closely-spaced fractures and shatter cones were not formed during shock compression, as widely postulated in the past, but immediately after the passage of the shock wave, by the interference of the scattered elastic wave and the tensional hoop stress that develops behind the shock front.

In addition to shatter cones, quartzite units show two other fracture types – a centimetre-spaced rhomboidal to orthogonal type that may be the product of shock-induced deformation and related to the formation of shatter cones, and later joints accomplishing tangential and radial extension. The occurrence of pseudotachylitic breccia within some of these later joints confirms the general impact timing of these features.

Pseudotachylitic breccias in the collar rocks occur as up to several centimetre-wide veins with variable orientations to the bedding and as more voluminous pods and networks in zones of structural complexity, such as the hinges of large-scale folds and along large-scale faults, as well as locally, at lithological interfaces. In places,

tension gash arrays along thin veins are observed indicating that movement occurred along these planes. Initial cooling calculations for pseudotachylitic breccias of different widths and compositions (metapelite or quartzite) suggest that thick veins (<10 cm) could have stayed molten over the entire duration of crater development (at least 10 minutes), making it possible for shock-induced melts to intrude dilational sites, such as fold hinges and extensional fractures, during the formation and subsequent collapse of the central uplift. Intrusion of such melts may also have lubricated movements along brittle and ductile structures. Thus, the presence of both shock- and friction-generated melts is likely in the collar of the Vredefort Dome.

Based on the spatial and geometric relationship between the structures and other deformation features observed in the collar rocks of the Vredefort Dome, it is possible to establish a temporal sequence of deformation events. Shatter cones and related closely-spaced fractures were formed during the contact/compression phase of the cratering process. The formation of at least some shock-induced pseudotachylitic breccia also belongs into this phase. Large-scale folds and faults and friction-generated melts can be related to the initial formation of the central uplift and extensional joints to the subsequent collapse of the central uplift.

Acknowledgements

I would like to thank my supervisors Prof. Wolf Uwe Reimold and Prof. Roger Gibson for giving me the opportunity to come to South Africa and to carry out this project. Their doors were always open, whenever I had questions or needed access to material or data, and they provided thoughtful input and important discussions of this project.

Besides my supervisors, who provided funding for this project, I am also grateful to the National Geographic Society, The Barringer Family Fund for Meteorite Impact Research, and the Geological Society of South Africa for financial support. Paula Ogilvie provided valuable data for the cooling calculations. Furthermore, I would like to thank the Chief Directorate of Mapping in South Africa, the De Beers Mining Company, especially Craig Smith and Stuart MacGregor, also Lynda Whitfield, Diane du Toit, Alex Mathebula, Henya Czekanowska, Gordon Cooper, Matt Kitching and Mitch Miles for technical support and assistance in analytical and imaging matters. I am also very grateful to the numerous landowners in the Vredefort area, who not only granted access to their properties but also showed generous hospitality during my extensive field work; in particular, Johannes van der Merwe and family at Thabela Thabeng, Dewald and Sandra Venter, and the family Oppermann.

In addition, I am grateful to everybody at the School of Geosciences at the University of the Witwatersrand, who was willing to listen to my numerous questions, and who spent some of their valuable time to discuss problems with me and, thus, contributed to my project.

Thanks also to everybody at the Ruprecht-Karls University in Heidelberg, Germany, in particular Anja Schleicher and Prof. R.O. Greiling, who provided much needed support in order for me to finish my project in Germany and to stay in touch with my supervisors in South Africa.

Last, but not least, I would like to express my most sincere appreciation to all friends and family members in South Africa and Germany who supported me and helped me out whenever needed; most special thanks to Mwamba Malama and her family for their great patience and support.

Contents

Chapter 1: Introduction

1.1 Purpose of study.....	1
1.2 Research history of Impact Cratering.....	3
1.3 Identification of impact structures.....	6
1.3.1 Geophysical and macro-deformation signatures.....	7
1.3.2 Shock deformation features.....	8
1.4 Crater morphology.....	12
1.5 Mechanics of formation of complex impact structures.....	16
1.6 Remaining problems regarding the Vredefort Dome.....	18
1.7 Geology and evolution of the Witwatersrand Basin.....	21
1.7.1 Geological Setting of the Witwatersrand Basin.....	21
1.7.1.1 <i>Dominion Group</i>	25
1.7.1.2 <i>Witwatersrand Supergroup</i>	25
1.7.1.3 <i>Ventersdorp Supergroup</i>	29
1.7.1.4 <i>Transvaal Supergroup</i>	30
1.7.1.5 <i>Post-Transvaal sedimentation and tectonic activity</i>	31
1.8 The Vredefort impact structure.....	33
1.9 Previous work on the Vredefort impact structure.....	38
1.9.1 Models for the formation of the Vredefort Dome.....	38
1.9.2 Petrographic work.....	40
1.9.3 Metamorphic studies.....	41
1.9.4 Structural studies in and around the Vredefort impact structure.....	44
1.10 Methodology.....	48

Chapter 2: Deformation structures in the collar of the Vredefort Dome

2.1 Introduction.....	54
2.2 Structural setting of the collar of the Vredefort Dome.....	55
2.3 Megascopic impact-related deformation features.....	62
2.4 Gross collar morphology.....	62
2.4.1 Tangential shortening of the collar strata.....	64
2.5 Folds.....	68
2.5.1 Fold A.....	69
2.5.2 Fold B.....	72
2.5.3 Fold C.....	74
2.5.4 Fold D.....	79
2.5.5 Fold E.....	82
2.5.6 Other folds in the collar of the Vredefort Dome.....	84
2.6 Faults.....	87

2.6.1 Shear zones.....	95
2.7 Joints and shear fractures.....	104
2.8 Synthesis of data.....	116

Chapter 3: Shatter cones

3.1 Introduction.....	119
3.2 Background.....	121
3.2.1 General observations on shatter cones.....	121
3.2.2 Previous observations on shatter cones at Vredefort.....	122
3.2.3 Hyptheses on shatter cone formation.....	125
3.2.3.1 <i>Overview of past hypotheses</i>	125
3.2.3.2 <i>Recent hypotheses: Baratoux and Melosh (2003)</i>	126
3.2.3.3 <i>Sagy et al. (2002, 2004)</i>	127
3.3 Methodology for this study.....	132
3.4 Results.....	135
3.4.1 Distribution and occurrence of shatter cones in the collar of the Vredefort Dome and environs.....	135
3.4.2 Shatter cone morphology.....	141
3.4.3 Striation geometries.....	146
3.4.4 Shatter cone orientation.....	148
3.4.5 Striation angles.....	154
2.5 Summary.....	158

Chapter 4: Pseudotachylitic breccias, other breccias and veins

4.1 Introduction.....	161
4.2 Previous work.....	162
4.2.1 Classification of pseudotachylitic breccias in impact structures.....	164
4.2.2 Occurrence and timing of pseudotachylitic breccias in the Vredefort Dome.....	165
4.2.3 Geochemical and petrographic observations of pseudotachylitic breccias	168
4.3 Observations on pseudotachylitic breccias during this study.....	171
4.3.1 Distribution of pseudotachylitic breccias.....	171
4.3.2 Morphology of pseudotachylitic breccias.....	172
4.3.2.1 <i>Pseudotachylitic breccias in quartzite units</i>	175
4.3.2.2 <i>Pseudotachylitic breccias in metapelite units</i>	176
4.3.3 Structural relationships of pseudotachylitic breccias with other structures in the collar strata.....	180
4.4 Timing of breccia formation.....	185
4.4.1 Cooling times for pseudotachylitic breccias.....	189
4.4.2 Results for melts with an initial temperature of 2000°C	192
4.4.3 Results for melts with initial melt temperature of 1400°C	197

4.4.4 Results for melts with initial melt temperature of 1000°C.....	198
4.4.5 Synthesis of data.....	200
4.5 Occurrence of other veins and breccias.....	204
4.5.1 Quartz veins.....	204
4.5.2 Other breccias.....	205
4.5.3 Synthesis of data.....	209

Chapter 5: Deformation in the outer parts of the Vredefort impact structure

5.1 Introduction.....	211
5.2 Regional Overview.....	211
5.3 Previous structural work in the wider environs of the Vredefort Dome.....	214
5.4 This study.....	222
5.4.1 Spitskop Syncline.....	224
5.4.2 Brecciation.....	226
5.4.3 Thrust faults.....	229
5.4.3.1 <i>Section 1</i>	232
5.4.3.2 <i>Section 2</i>	234
5.4.3.3 <i>Section 3</i>	234
5.4.3.4 <i>Section 4</i>	237
5.4.4 Extensional faults.....	241
5.4.5 The Losberg Complex.....	247
5.5 Synthesis of data.....	251

Chapter 6: Discussion

6.1 Introduction.....	253
6.2 The deformation of the collar rocks.....	253
6.2.1 Faults and Folds.....	254
6.2.1.1 <i>Stress pattern responsible for the formation of impact-related folds and faults</i>	255
6.2.1.2 <i>Kinematic indicators</i>	257
6.2.1.3 <i>Tangential shortening</i>	261
6.2.2 Implications for central uplift formation and cratering mechanics.....	263
6.2.2.1 <i>Formation of central uplift</i>	263
6.2.2.2 <i>Collapse of the central uplift</i>	267
6.2.2.3 <i>Deformation in the outer parts of the Vredefort impact structure</i>	270
6.2.3 Joints and shear fractures.....	273
6.2.4 Shatter cones.....	275
6.2.4.1 <i>Distribution and occurrence of shatter cones in the Vredefort Dome</i>	275
6.2.4.2 <i>Shatter cone morphology</i>	275
6.2.4.3 <i>Striation geometries</i>	276

6.2.4.4 Shatter cone orientation.....	278
6.2.4.5 Relationships of shatter cones to other deformation features.....	280
6.2.4.6 Genesis of shatter cones.....	283
6.2.5 Pseudotachylitic breccias.....	286
6.3 Chronology of impact-related deformation.....	291
6.3.1 Contact/compression phase.....	291
6.3.2 Formation of central uplift.....	293
6.3.3 Collapse of central uplift.....	295
6.3.4 Gravitational adjustment.....	296
6.4 Further work.....	296
6.5 Summary and conclusions.....	297
Reference list.....	302

Reference list for reprinted figures.....	343
--	------------

Appendix (on CD-Rom).....	345
Appendix 1 (Flight information of Landsat images and aerial photographs.....)	346
Appendix 2 (Location Maps).....	348
Appendix 3 (Description of selected thin sections).....	352
Appendix 4 (Results for cooling calculations for pseudotachylitic breccias).....	355
Appendix 5 (Shatter cone measurements).....	395
Appendix 6 (Data list).....	397
Appendix 7 (Published abstracts and papers).....	497

List of Figures

Fig. 1.1: Simple crater on the Moon.....	5
Fig. 1.2: Complex crater on the Moon.....	6
Fig. 1.3: Pressure-temperature diagram for shock metamorphism.....	10
Fig. 1.4: Formation of a simple crater.....	13
Fig. 1.5: Formation of a complex crater.....	14
Fig. 1.6: Schematic maps of the Kaapvaal Craton, the Witwatersrand Basin and the Vredefort Structure.....	22
Fig. 1.7: Evolution models for the Witwatersrand Basin.....	24
Fig. 1.8: Stratigraphic column of the Witwatersrand Basin.....	26
Fig. 1.9: Stratigraphic column of the Witwatersrand Supergroup.....	28
Fig. 1.10: Distribution of faults and folds in the Witwatersrand Basin prior to the impact.....	29
Fig. 1.11: Distribution and occurrences of intrusives in the Vredefort Dome.....	32
Fig. 1.12: Landsat TM image of the Vredefort impact structure.....	35
Fig. 1.13: Interpretative structural map of the area around the Vredefort Dome (after Brink et al., 2000a).....	36
Fig. 1.14: Distribution of lithologies and structures around the Vredefort Dome (after McCarthy et al. 1990).....	37
Fig. 1.15: Models of formation for the Vredefort Dome.....	39

Fig. 1.16: Eccentric distribution of the pre-impact metamorphic isograd in the Vredefort Dome....	42
Fig. 1.17: Explanation for the eccentric distribution of the metamorphic isograd after Lana et al. (2003a).....	43
Fig. 1.18: Vredefort Granophyre.....	47
Fig. 1.19: Interpretative cross-section through the Witwatersrand Basin (after Friese et al. 1995)...	49
Fig. 1.20: Landsat image with a TM 321 true colour combination of the Vredefort Dome.....	51
Fig. 1.21: Schematic map of the exposed collar strata in the Vredefort Dome.....	52
Fig. 2.1: Simplified geological maps of the Witwatersrand Basin and the Vredefort Dome.....	56
Fig. 2.2: Block fault model for the formation of the Vredefort sub-basin (after Holland et al. 1990)	58
Fig. 2.3: Landsat-TM image of the Vredefort Dome showing the pre-impact faults in the collar.....	59
Fig. 2.4: Scissor-type rotation of megablocks (after Albat 1988).....	59
Fig. 2.5: Map of the core of the Vredefort Dome divided into six segments after Lana et al. (2003a).....	61
Fig. 2.6: Combined aerial photographs of the northern collar.....	63
Fig. 2.7: Orientation analysis of collar strata.....	65
Fig. 2.8: Metre-scale fold in the northwestern collar.....	68
Fig. 2.9: Decametre-scale fold in the northwestern collar.....	70
Fig. 2.10: Large-scale symmetric and asymmetric folds in the collar of the Vredefort Dome.....	71
Fig. 2.11: Structural analysis of Fold A.....	73
Fig. 2.12: Structural analysis of Fold B.....	75
Fig. 2.13: Photographs of Fold C in the northwestern collar.....	77
Fig. 2.14: Structural analysis of Fold C.....	78
Fig. 2.15: Photographs of hinge zone of Fold C.....	80
Fig. 2.16: Structural analysis of Fold D.....	81
Fig. 2.17: Structural analysis of Fold E.....	83
Fig. 2.18: Decametre-scale fold in the northeastern collar.....	85
Fig. 2.19: Fold structure in the northern outer collar.....	86
Fig. 2.20: Aerial photographs of large-scale faults in the collar.....	88
Fig. 2.21: Rose diagrams of major faults in the collar strata.....	89
Fig. 2.22: Photograph on slickensides on bedding surface.....	91
Fig. 2.23: Photograph of a pseudotachylitic breccia vein with oblique orientation with regard to the bedding.....	93
Fig. 2.24: Photograph of block rotation in the western collar.....	94
Fig. 2.25: Photograph of exposed Booyens Shale Formation along a road-cut.....	97
Fig. 2.26: Photograph of road-cut and analysis of structures.....	98
Fig. 2.27: Photograph of asymmetric lens in a shale unit in the northern collar.....	100
Fig. 2.28: Photograph of a shear zone in a quartzite unit near Fold E.....	101
Fig. 2.29: Microphotographs of the shear band cleavage.....	103
Fig. 2.30: Photographs of small-scale faults in a metapelitic unit in the northern collar.....	105
Fig. 2.31: Photograph of a conjugate set of fractures in metapelitic rocks in the northern collar.....	106
Fig. 2.32: Photograph of closely spaced sets of joints in metapelites in the northwestern collar.....	107
Fig. 2.33: Photograph and structural analysis of joints in quartzite in the northwestern collar.....	108
Fig. 2.34: Photograph of bedding-parallel fractures in the northern collar.....	109
Fig. 2.35: Photograph of strongly curved fractures in the collar strata.....	110
Fig. 2.36: Photograph of radial, subvertical joints (set I) in the collar rocks.....	111
Fig. 2.37: Photograph of conjugate joints/shear fractures in the collar rocks.....	112
Fig. 2.38: Photograph of shear planes in a shale unit in the northern collar.....	114
Fig. 2.39: Structural analysis of fractures in quartzites and alkali granites.....	115
Fig. 3.1: Photograph of a conical shatter cone from the Houghton Structure, Canada.....	120
Fig. 3.2: Photograph of a shatter cone with curved striations.....	120
Fig. 3.3: Photograph of sets of closely-spaced fractures in alkali granite , northern collar.....	124
Fig. 3.4: Illustration of the formation of shatter cones after Baratoux and Melosh (2003).....	126
Fig. 3.5: Stress history of a shock wave at a heterogeneity (after Baratoux and Melosh 2003).....	128

Fig. 3.6: Characteristics of fracture front waves (after Sagy et al. 2004).....	129
Fig. 3.7: V-shaped striation angles on shatter cones (after Sagy et al. 2004).....	130
Fig. 3.8: Diagram of V angles of shatter cone striations in the Vredefort Dome (after Sagy et al. 2004).....	131
Fig. 3.9: Schematic map of shatter cone sites in the Vredefort Dome.....	136
Fig. 3.10: Photograph of striated surfaces at a road-cut in the northwestern collar.....	137
Fig. 3.11: Photograph of striated surfaces in the outer parts of the Vredefort structure.....	139
Fig. 3.12: Photograph of curved striations on a shatter cone segment in the collar rocks.....	140
Fig. 3.13: Photographs of shatter cones of different sizes.....	142
Fig. 3.14: Photographs of typical shatter cone morphology in the collar of the Vredefort Dome....	143
Fig. 3.15: Photographs of examples of shatter cones with subparallel striations.....	144
Fig. 3.16: Microphotographs of fractures in a shatter cone sample from the northern collar.....	145
Fig. 3.17: Photographs of shatter cone apices with different orientations.....	147
Fig. 3.18: Photographs of shatter cone apices with different orientations to bedding.....	149
Fig. 3.19: Stereonets of shatter cone striations and fractures from different locations in the collar:	
(a) location 2.....	150
(b) location 149.....	151
(c) location 680.....	152
Fig. 3.20: Photograph of fractures cutting shatter cones from the northwestern collar.....	154
Fig. 3.21: Photographs of horsetail structures on shatter cone surfaces.....	155
Fig. 3.22: Striation angles on a shatter cone segment from the northwestern collar.....	156
Fig. 3.23: Statistical evaluation of mean striation angle widths from different locations.....	157
Fig. 3.24: Mean angle width of striation with distance from the centre.....	159
Fig. 4.1: Typical appearance of massive pseudotachylitic breccia in the core of the Vredefort Dome.....	167
Fig. 4.2: Microscopic flow textures in pseudotachylitic breccias.....	169
Fig. 4.3: Microphotograph of pseudotachylitic breccia.....	170
Fig. 4.4: Photograph of pseudotachylitic breccia occurrence in the outer collar.....	171
Fig. 4.5: Pods and networks of pseudotachylitic breccias in hinge zones of large-scale folds.....	173
Fig. 4.6: Pseudotachylitic breccia occurrence close to a large-scale fault.....	174
Fig. 4.7: Photographs of pseudotachylitic breccias parallel and oblique to bedding.....	176
Fig. 4.8: Pseudotachylitic breccia occurrence in a kink band in metapelitic rocks.....	178
Fig. 4.9: Photographs of fractures filled with pseudotachylitic breccia.....	179
Fig. 4.10: Photographs of flow textures in pseudotachylitic breccias.....	181
Fig. 4.11: Photograph of en echelon tension gashes along bedding-parallel pseudotachylitic breccia vein.....	182
Fig. 4.12: Aerial photograph of drag-folding along a radial large-scale fault in the northeastern collar.....	183
Fig. 4.13: Photograph of a thin pseudotachylitic breccia vein cut by shear fractures.....	184
Fig. 4.14: Microphotograph of fractures cutting through a cm-wide pseudotachylitic breccia vein..	185
Fig. 4.15: Photograph of crosscutting pseudotachylitic breccia veins.....	187
Fig. 4.16: Cooling temperatures for 1 mm wide veins with initial melt T of 2000°C.....	193
Fig. 4.17: Cooling temperatures for 1 cm wide veins with initial melt T of 2000°C.....	194
Fig. 4.18: Cooling temperatures for 10 cm wide veins with initial melt T of 2000°C.....	195
Fig. 4.19: Cooling temperatures for 1 mm wide veins with initial melt T of 1400°C.....	198
Fig. 4.20: Cooling temperatures for 1 and 10 cm wide veins with initial melt T of 1400°C.....	199
Fig. 4.21: Cooling temperatures for 1 mm wide veins with initial melt T of 1400°C.....	200
Fig. 4.22: Cooling calculations for 1 cm and 10 cm veins with initial melt T of 1000°C.....	202
Fig. 4.23: Typical occurrence of millimetre-wide quartz veins in the collar of the Vredefort Dome.	204
Fig. 4.24: Schematic map of the exposed collar rocks showing the orientation of quartz veins in the collar.....	206
Fig. 4.25: Photograph of quartz vein crosscut by shear fractures.....	207
Fig. 4.26: Photograph of quartz-hosted breccia in the northeastern collar.....	208
Fig. 4.27: Photograph of quartz clasts and matrix of quartz-hosted breccia.....	208

